Supplementary Materials for

An extremely bright gamma-ray pulsar in the Large Magellanic Cloud

The *Fermi*-LAT collaboration*

* Corresponding author. E-mail: pierrick.martin@irap.omp.eu; lucas.guillemot@cnrs-orleans.fr; francis.e.marshall@nasa.gov

This PDF file includes:

S1 Materials and Methods

S1.1 Large Area Telescope data analysis

The complete LMC emission model was determined using a maximum-likelihood model-fitting approach. Typically, a model consists of several emission components and has a certain number of free parameters. A distribution of expected counts in position and energy is obtained by convolution of the model with the instrument response functions, which includes the energy-dependent point spread function, taking into account the exposure achieved for the data set that is used. Free parameters are adjusted in an iterative way until the distribution of expected counts provides the highest likelihood of the data given the model.

A complete spatial and spectral emission model for the $10^\circ \times 10^\circ$ region encompassing the LMC was derived from 73 months of *Fermi*-LAT Pass 7 Reprocessed data (*27*). The LMC model consists of a large-scale extended component spanning about the angular size of the galaxy, three smaller-scale extended components with sizes of order 1–2°, and four point sources. Two possibilities were considered for the modelling of extended emission from the LMC: 2D Gaussian gamma-ray intensity distributions, and a physical model in which emission arises from the interaction of localized populations of cosmic rays with interstellar gas. The latter option provides the model with the highest likelihood and satisfactory residuals after subtraction of the model from the data.

Based on this emission model, the spectral properties of the various sources in the LMC were updated with 75 months of Pass 8 data, using a preliminary internal version of the data and the corresponding instrumental response functions. As for the Pass 7 Reprocessed data analysis, we considered events of the so-called 'Source' class (as recommended by the *Fermi*-LAT collaboration for the analysis of point sources and Galactic diffuse emission), with reconstructed energies in the 0.2–100 GeV range. All event types of the SOURCE class were included: con-

version in the front and back sections of the tracker, and all qualities of reconstructed energy and direction. We focus below on the two sources that are the main point of the article.

Using the whole set of Pass 8 data, PSR J0540−6919 is detected with a test statistic of 307 (for the definition of the test statistic, see (*41*)), corresponding to a detection at the 17σ confidence level for 3 degrees of freedom (the spectral parameters of the power law with exponential cutoff model). While significant pulsations were already detected with Pass 7 reprocessed data, using Pass 8 data resulted in an increase of nearly 2σ in the significance of the pulsations. This results primarily from the $\sim 25\%$ increase in acceptance at 1–10 GeV energies.

Restricting the analysis to the time interval over which we have a valid rotation ephemeris for PSR J0540−6919 (see below), we have performed a phase-resolved study by splitting the rotation period into two phase intervals, on-pulse and off-pulse, the latter being conservatively defined as the 0.3–0.8 phase range. In the on-pulse interval, PSR J0540−6919 is detected at the 11σ level and its spectrum can be described as a power law with photon index 2.0 ± 0.2 and an exponential cutoff at 5.2 ± 2.1 GeV. In the off-pulse interval, PSR J0540−6919 is detected at the 4.7σ level, and its spectrum can be described as a simple power law with photon index 2.5 ± 0.1 (while being consistent with the power-law with exponential cutoff models of the on-pulse interval and full data set). The corresponding spectra are presented in Fig. S1.

Using Pass 8 data, the source coincident with PSR J0537−6910 is detected with a test statistic of 127, corresponding to a 11σ detection for 4 degrees of freedom (the spectral parameters of the power law model and the position parameters). The spectrum of the source can be described as a simple power law with photon index 2.1 ± 0.1, which is consistent with the results obtained from the analysis of Pass 7 reprocessed data (*27*). Such a flat spectrum with significant emission above 20 GeV is not typical of young pulsars and may result from the superposition of weakly modulated pulsar emission with radiation from the associated pulsar wind nebula and/or supernova remnant. The energy flux above 100 MeV is $h = (1.4 \pm 0.2) \times 10^{-11}$ erg cm^{-2} s^{-1}.

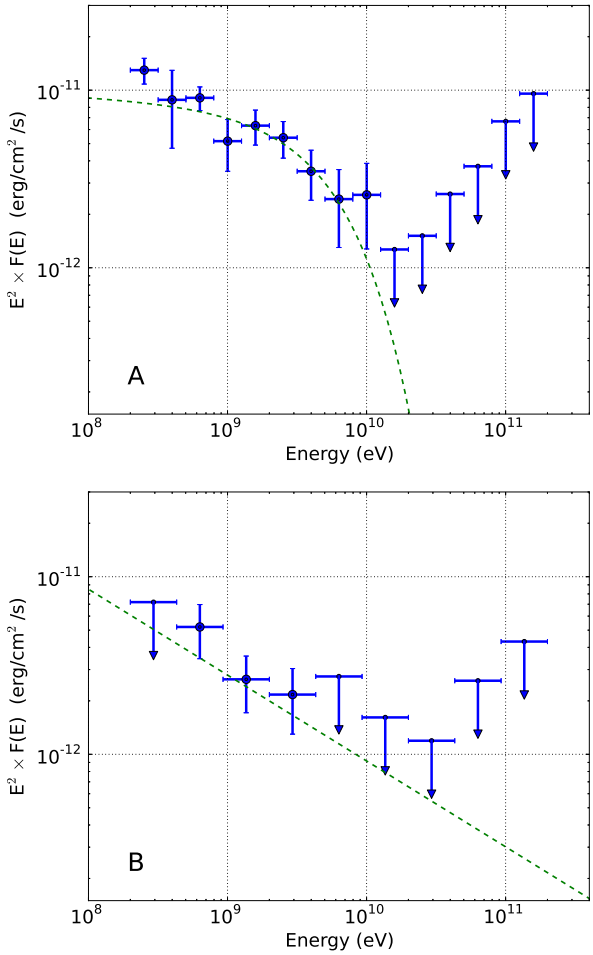

Figure S1: **Phase-resolved gamma-ray spectra of PSR J0540−6919.** (A) On-pulse phase interval. (B) Off-pulse phase interval. Upper limits correspond to a 95% confidence level. The dashed green lines show the best-fit models.

For the determination of an upper limit on the pulsed emission from PSR J0537−6910, we also quote the energy flux between 100 MeV and 10 GeV, $h = (1.1 \pm 0.2) \times 10^{-11}$ erg cm^{-2} s^{-1}.

S1.2 Rotation ephemerides for PSR J0540−6919 and PSR J0537−6910

The *Fermi* Large Area Telescope (LAT) gamma-ray data and the Iqueye photometer optical data considered in our study were phase-folded with a rotation ephemeris for PSR J0540−6919

based on Rossi X-ray Timing Explorer (RXTE) observations recorded between MJD 54602 (2008 May 16) and 55898 (2011 December 3). The solution uses the optical pulsar position, $\alpha_{\rm J2000}$ = $05^h40^m11.202^s$ and $\delta_{\rm J2000}$ = $-69°19'54.17''$ (*29*), and models the period and period derivative in intervals separated by two small discontinuities at MJDs 54966.4 and 55487.3 added to account for the data adequately. The resulting timing model predicts arrival times to 0.7 ms or 0.014 in pulsar phase. The timing parameters are listed in Table S1.

RXTE observations also provide an accurate ephemeris for PSR J0537−6910 valid from MJD 54774 (4 November 2008) to 55701 (20 May 2011), using the pulsar X-ray position $\alpha_{\rm J2000}$ = $05^h37^m47.36^s$, and $\delta_{\rm J2000}$ = $-69°10'20.4''$ (*42*). Similarly to PSR J0540−6919, the solution models the period in intervals separated by small discontinuities. The timing model predicts arrival times to an accuracy of 0.2 ms or 0.014 in pulsar phase. The solution is given in Table S2.

S1.3 Upper limit on the pulsed luminosity of PSR J0537−6910

Analysis of the LAT data revealed a significant gamma-ray source at a position coincident with PSR J0537−6910. Its spectrum is consistent with a simple power law extending to about 50 GeV without evidence for a cutoff characteristic of pulsar magnetospheric emission. We nevertheless searched for pulsations from PSR J0537−6910 and failed to detect any pulsed signal with significance larger than 1σ, suggesting that strongly pulsed emission is at most a small fraction of the total signal from the source.

In order to determine an upper limit on the pulsed luminosity of PSR J0537−6910, we selected LAT photons found within 5° of the pulsar and having energies 0.1–10 GeV, and we assigned these photons probabilities that they originated from PSR J0537−6910, based on the emission model for the LMC. A Monte Carlo analysis was then performed in which for 100 logarithmically-spaced values of the pulsed fraction $p_{\rm frac}$ (where $p_{\rm frac}$ is the fraction of photons in the dataset contributing to the pulsed emission) between 10^{-3} and 1, we simulated 1000

realizations of a Gaussian-shaped profile for the pulsed emission containing $N_{\rm psr} = p_{\rm frac} \times N$ photons (where N denotes the total number of photons in the dataset) and $N_{\rm bkgd} = N - N_{\rm psr}$ background photons with random phases. A full width at half maximum of 10% of the pulsar rotation was used for the simulated gamma-ray profile, similar to the X-ray profile of PSR J0537−6910 (*11*). For each realization, $N_{\rm psr}$ values of the spectral weights were selected at random from the actual dataset, and the remaining spectral weights were randomly assigned to the other $N_{\rm bkgd}$ photons. Finally, we calculated the weighted H-test parameter at each step, and determined the fraction of $> 5\sigma$ detections among the 1000 realizations, for each $p_{\rm frac}$ value.

The conclusion from the Monte Carlo analysis was that any value of $p_{\rm frac}$ larger than ~ 0.06 results in highly significant detections in at least 95% of cases. This value of $p_{\rm frac}$ can therefore be used to place an upper limit on the pulsed luminosity of PSR J0537−6910. With a total 0.1–10 GeV luminosity for the source coincident with PSR J0537−6910 of $L_{\gamma,\ \rm J0537} = 3.1 \times 10^{36}$ erg s^{-1} (*27*), we obtain a limit of $p_{\rm frac} \times L_{\gamma,\ \rm J0537} \sim 1.9 \times 10^{35}$ erg s^{-1}.

Parameter	Value
Right Ascension, $\alpha_{\rm J2000}$	$05^h40^m11.202^s$
Declination, $\delta_{\rm J2000}$	$-69°19'54.17''$
Reference Epoch (MJD)	54792.81555049109
Spin Frequency, ν (Hz)	19.74426902754
First Time Derivative of ν, $\dot{\nu}$ (10^{-10} Hz s^{-1}) ..	-1.8667600
Second Time Derivative of ν, $\ddot{\nu}$ (10^{-21} Hz s^{-2})	3.7502
Epoch of Discontinuity 1 (MJD)	54966.4266616022
Increment in Rotational Phase	0.005
Increment in ν (Hz)	-0.56×10^{-8}
Increment in $\dot{\nu}$ (10^{-10} Hz s^{-1})	2×10^{-6}
Increment in $\ddot{\nu}$ (10^{-21} Hz s^{-2})	0.054
Epoch of Discontinuity 2 (MJD)	55487.25999493553
Increment in Rotational Phase	0.010
Increment in ν (Hz)	-1.96×10^{-8}
Increment in $\dot{\nu}$ (10^{-10} Hz s^{-1})	2.74×10^{-5}
Increment in $\ddot{\nu}$ (10^{-21} Hz s^{-2})	-0.283
Solar System Ephemeris	DE200
Reference Time Scale	TDB
Validity Range (MJD)	54602 – 55898
RMS Timing Residuals (ms)	0.7

Table S1: Timing parameters for PSR J0540−6919.

Parameter	Value
Right Ascension, $\alpha_{\rm J2000}$	$05^h37^m47.36^s$
Declination, $\delta_{\rm J2000}$	$-69°10'20.4''$
Reference Epoch (MJD)	54677.07480975035
Spin Frequency, ν (Hz)	61.9815193952
First Time Derivative of ν, $\dot{\nu}$ (10^{-10} Hz s^{-1}) ..	-1.994664
Second Time Derivative of ν, $\ddot{\nu}$ (10^{-21} Hz s^{-2})	9.6
Epoch of Discontinuity 1 (MJD)	54711.79703197257
Increment in Rotational Phase	0.090
Increment in ν (Hz)	6.5921×10^{-6}
Increment in $\dot{\nu}$ (10^{-10} Hz s^{-1})	-0.716×10^{-3}
Epoch of Discontinuity 2 (MJD)	54769.66740234294
Increment in Rotational Phase	0.696
Increment in ν (Hz)	22.4152×10^{-6}

Continued on next page

Parameter	Value
Increment in $\dot{\nu}$ (10^{-10} Hz s^{-1})	-0.846×10^{-3}
Epoch of Discontinuity 3 (MJD)	54885.40814308368
Increment in Rotational Phase	0.741
Increment in ν (Hz)	21.2181×10^{-6}
Increment in $\dot{\nu}$ (10^{-10} Hz s^{-1})	-1.004×10^{-3}
Epoch of Discontinuity 4 (MJD)	55041.65814308368
Increment in Rotational Phase	0.378
Increment in ν (Hz)	13.4614×10^{-6}
Increment in $\dot{\nu}$ (10^{-10} Hz s^{-1})	-1.563×10^{-3}
Increment in $\ddot{\nu}$ (10^{-21} Hz s^{-2})	11.3
Epoch of Discontinuity 5 (MJD)	55182.86184678738
Increment in Rotational Phase	0.582
Increment in ν (Hz)	13.0182×10^{-6}
Increment in $\dot{\nu}$ (10^{-10} Hz s^{-1})	-2.6679×10^{-3}
Epoch of Discontinuity 6 (MJD)	55267.35258752813
Increment in Rotational Phase	0.300
Increment in ν (Hz)	34.0678×10^{-6}
Increment in $\dot{\nu}$ (10^{-10} Hz s^{-1})	-1.241×10^{-3}
Increment in $\ddot{\nu}$ (10^{-21} Hz s^{-2})	-14.17
Epoch of Discontinuity 7 (MJD)	55452.53777271331
Increment in Rotational Phase	0.643
Increment in ν (Hz)	10.4278×10^{-6}
Increment in $\dot{\nu}$ (10^{-10} Hz s^{-1})	-0.867×10^{-3}
Epoch of Discontinuity 8 (MJD)	55452.53777271331
Increment in Rotational Phase	0.900
Increment in ν (Hz)	7.6476×10^{-6}
Increment in $\dot{\nu}$ (10^{-10} Hz s^{-1})	-0.420×10^{-3}
Epoch of Discontinuity 9 (MJD)	55556.70443937997
Increment in Rotational Phase	0.122
Increment in ν (Hz)	0.6292×10^{-6}
Increment in $\dot{\nu}$ (10^{-10} Hz s^{-1})	0.730×10^{-3}
Epoch of Discontinuity 10 (MJD)	55585.639624565163
Increment in Rotational Phase	0.027
Increment in ν (Hz)	5.4499×10^{-6}
Increment in $\dot{\nu}$ (10^{-10} Hz s^{-1})	-1.800×10^{-3}
Epoch of Discontinuity 11 (MJD)	55614.574809750346
Increment in Rotational Phase	0.156
Increment in ν (Hz)	28.1097×10^{-6}

Continued on next page

Parameter	Value
Increment in $\dot{\nu}$ (10^{-10} Hz s^{-1})	0.057×10^{-3}
Solar System Ephemeris	DE200
Reference Time Scale	TDB
Validity Range (MJD)	$54774 - 55701$
RMS Timing Residuals (ms)	0.2

Table S2: Timing parameters for PSR J0537−6910.